Implementation of the Lumped-Oscillator Model (LOM) on a Tunable Coupler for Superconducting Qubits Using Qiskit Metal

Sarah Dweik

A report submitted in partial fulfilment of the requirements for the passing PHYS411

Advisor: Prof. Abdallah Sayyed' Ahmad

February 26, 2025

Acknowledgement

"I would like to express my sincere gratitude to Dr. Muhammad Waqar Amin from PIEAS, and his student Risav Pokhrel, for their invaluable assistance in compiling part of the Qiskit Metal code that I was unable to run due to unlicensed Ansys. I also wish to thank my colleague, Mohamad Abdalhadi, from the Electrical Engineering Department at Birzeit University, for his efforts in refining the circuit schematic of the Tunable Coupler that I utilized in my research. My deepest appreciation goes to my advisor, Prof. Abdallah Sayyed Ahmad, for his guidance, patience, and unwavering support throughout my studies and research. Finally, I would like to extend my heartfelt thanks to my family and friends for their constant encouragement, kind words, and assurance during this journey. "

Contents

List of Figures

List of Source Code

Chapter 1

Introduction and Background

1.1 Introduction

Superconducting Qubits are at the forefront of the Quantum Computers industry. And is believed to have taken over the first operational system. One recent example is the 2024 "Tianyan-504" superconducting Quantum computer, which features 504 Qubits, the largest number of Qubits on a chip so far! However, the scalability of this technology is a critical challenge due to the errors of various origins, decoherence, measurement errors, gates errors, cross-talk, and others.

Many solutions have been developed to overcome such defects. On both software and hardware aspects. For instance, surface code, Stean code, and Bosonic code those error correction techniques that encode logical qubits into the given physical systems. On the other hand, arguably more important is engineering the processors themselves in such a way that mitigates the errors.

Developing and engineering Quantum processors isn't an easy process. Similar to the classical microchip manufacturing process, fabricating the Quantum chip is also complex and sources expensive. Hence, designing tools are critical; where simulation and optimization guarantee a chip with the aimed functionality. Luckily, Open-Quantum-Hardware is innovative, contributing to accelerating advancements in the Quantum Computing industry.

Simulating the full Quantum dynamic of the quantum process can be expensive. For example, ... A group from IBM developed the method Lumped Oscillator Model, LOM, which is a computationally efficient method that systematically builds the Quantum Hamiltonian, and extracts its properties from the Quantum Field.

This work focuses on applying this method to two coupled superconducting Qubits using Qiskit Metal and compares the check experimental agreement. The Qubit-Qubit coupler is a tunable coupler that was investigated in [2]

Dispersive shifts between Qubits should be able to imply results about the cross-talk between the two Qubits, and hence validate similarities between the theoretical and simulations outcome.

1.2 literature Review

1.2.1 Quantum Computers

The need for and importance of quantum processors arises when observing Moore's law, the co-founder of INTEL, who stated his historical observation of the growing rate of transistors on integrated circuits. Such that the number of transistors fabricated into the chip doubles every two years, consequentially, the size of the transistor should continually shrink! The average size of it is 10 nm according to the International Road-map For Devices And Systems.

The compressing process of size comes to a limit, and Quantum effects take over. Phenomenons like superposition and Entanglement are spotted. If those behaviors are correctly employed then they produce what is called Quantum Computer.

Computers in the classical, modern definition should be able to store data, transfer data, and carry out related tasks. Hence, not every quantum system can necessarily function as a quantum computer. DiVincenzo's criteria define when such a system can be operational and outperform the classical machines for certain assignments. The experimental setup must satisfy the following:

- Analogous to the binary bit. A quantum bit -Qubit- must be precisely identified for the physical system to be expandable.
- One must be able to initially set the Qubit in a reference state.
- The Qubit should be able to retain its Quantum behaviors for a relatively long time- Long coherence time-
- The states of the Qubit should be able to undergo certain transformations- Universal Quantum gates-
- One should be able to acquire information from the data stored and manipulated in Qubits - measurement-

There are multiple types of speculative Quantum Computers; because quantum dynamics exist in many systems of nature. For instance, trapped ion, photonic, spin, and superconducting Quantum Computers. These types primarily differ in the physical realization of the quantum bit (Qubit), with each system leveraging a unique method for encoding and manipulating information at the quantum level.

This work focuses on superconducting quantum computers, which are distinguishable from all other types. While the other types rely on the natural properties of quantum systems, superconducting quantum computers specifically rely on engineered quantum behaviors. As a result, they are more controllable, making superconducting quantum computers the most promising architecture.

1.2.2 Quantization of Lumped Models- QLM

QLM is the process of transitioning from the classical description of a circuit to a quantum description by addressing the quantum operators from conventional variables.

This section introduces the fundamental notation used in circuit quantum electrodynamics, a subfield of quantum electrodynamics tailored to superconducting quantum computers. It begins with an outline of the key concepts and describes the transition from a classical to a quantum description of circuits by deriving quantum operators from conventional variables.

Charge and flux across an electric circuit correspond to continuous values. While the charge is associated with movement and accumulation of charges.

$$I(t) = \frac{dQ(t)}{dt} \tag{1.1}$$

The flux describes the amount of magnetic field through the circuit.

$$\Phi(x,t) = \int_{-\infty}^{t} dt' V(x,t') \tag{1.2}$$

From Eq.2 it can be observed that flux is a relative quantity, and that it described as node-to datum. Thus it corresponds to the potential energy of the circuit. In contrast, the charge movements across the circuit indicates the Kinetic energy stored in the electric circuit configuration. This further implies an analogy between position x and $\Phi(x,t)$. and between momentum p and charge Q.

In a quantum regime, flux and charge obey canonical quantization, and act as conjugate variables. Undergoing Heisenberg uncertainty principle; it means that one can't conduct simultaneous measurements of the flux and charge.

$$[\hat{Q}, \hat{\Phi}] = i\hbar \tag{1.3}$$

To see how the charge is a conjugate momentum for the flux, a simple LC resonator is set to operate in the Quantum regime. By satisfying the following conditions conditions.

- High energy retaining, which can be done by large quality factor according to

$$Q = \frac{\text{Energy lost per cycle}}{\text{Energy stored in the circuit}}$$

- To maintain quantum properties, the system must not be dominated by heat. Thus, the energy gap between modes needs to be large enough compared to the energy associated with the temperature. $\hbar\omega \gg k_B T$

It was experimentally confirmed [15] that under these conditions, the LC resonator will undergo a quantized process. The charge build-up on the capacitor will be discrete. Flux values are discrete as well, giving rise to linearly separated eigenstates. So, the Hamiltonian is given by:

$$H = \frac{\hat{Q}^2}{2C} + \frac{\hat{\Phi}^2}{2L} \tag{1.4}$$

By analogy with position-momentum observables, flux, and charge operators can be represented using the creation and annihilation operators for convenience with dealing with the system as Quantum mechanical

$$\hat{H} = \frac{\hat{p}^2}{2m} + \frac{1}{2} m\omega^2 \hat{x}^2 \tag{1.5}$$

$$\hat{\Phi} = \Phi_{\text{zpf}}(\hat{a}^\dagger + \hat{a}), \quad \hat{Q} = iQ_{\text{zpf}}(\hat{a}^\dagger - \hat{a}) \tag{1.6}$$

Where the zero-point flux fluctuation is given by

$$\Phi_{\text{zpf}} = \sqrt{\frac{\hbar}{2\omega C}} \tag{1.7}$$

To generalize this analogy in the Quantization context. Quantized Canonical momentum is defined as follows according to [4]

$$Q(x, t) = c_0 \frac{\partial \Phi(x, t)}{\partial t} \tag{1.8}$$

1.2.3 Superconducting Quantum Computer

Superconducting materials are those that can shift into the superconductivity state at certain temperatures. Either at very high temperatures HTS like Yttrium Barium Copper Oxide YBCO. Or at very low temperatures LTS such as Niobium. In both scenrios, the material has two special characters. First, it shows zero resistance. Second, it repels any magnetic field- the Meissner effect.

Bardeen-Cooper-Shriefer (BCS) theory explains those remarks for LTS. At very low temperatures, vibrational degrees of freedom for the positive particle are frozen, so an electron travels without scattering, and it will attract them; shifting their positions slightly, thus, making the surrounding positively charged. When another electron passes it will be attached to this cloud enclosing the first electron. Those two electrons form the *Cooper pairs* the Fermions to act as Bosons, with a new ground state, which they all can habitat at once. This pair is a many-body

system that is more complex, so their wave-particle duality nature is not a Schrodinger Equation, rather it is described by The Landau -Ginsburg equations []

$$-\frac{\hbar^2}{2m^*}\nabla^2\Psi + a\Psi + b|\Psi|^2\Psi = 0 \tag{1.9}$$

The steady-state Ginzburg-Landau equation, in the absence of a magnetic field. where e is the elementary charge. And $\Psi(\mathbf{r})$ is the superconducting wavefunction, a and b are material-dependent parameters, and ∇^2 is the Laplacian operator. One possible solution- ansatz- for this equation

$$\Psi(\mathbf{r}) = |\Psi(\mathbf{r})|e^{i\theta(\mathrm{r})} \tag{1.10}$$

Josephson effect is one of the key phenomena enabled by superconducting material. *The structure* at which this effect is observed is two superconducting proximity plates separated by an insulator. Such a structure gives rise to *Super current* within the insulating gap, even when no external voltage is applied. Cooper pairs tunnel through the junction of anode and insulator. The **phase dependent** from Eq1.2 creates a voltage difference across the junction according to

$$\frac{d\Phi}{dt} = \frac{2\pi}{\Phi_0}V \tag{1.11}$$

The supercurrent flows according to:

$$I = I_c \sin(\varphi) \tag{1.12}$$

where I is the supercurrent, I_c is the critical current, and φ is the phase difference across the junction.

As a result, the Josephson junction inductance is phase dependent base on

$$\Phi = LI \tag{1.13}$$

The Josephson inductance is given by:

$$L_J(\Phi) = \left(\frac{\partial I}{\partial \Phi}\right)^{-1} = \frac{\Phi_0}{2\pi I_c}\frac{1}{\cos\left(\frac{2\pi\Phi}{\Phi_0}\right)} \tag{1.14}$$

Intrinsic junction's properties

The critical current and number of cooper pairs across the junction define two main traits of the Josephson junction. Those are energy junction E_j and charging energy E_c. Being intrinsic properties one might expect that they depend only on the geometrical factors. However, they are affected also by the current passing through the junction, according to

$$E_J = \frac{\hbar I_c}{2e} \tag{1.15}$$

$$E_C = \frac{e^2}{2C_\mathrm{j}} \tag{1.16}$$

I_c is the critical current, and capacitive effect is due to the proximity of the two superconducting plates.

These two qualities have two importance. First, together they specify the Qubit frequency that it uses the junction

$$\hbar\omega_{01} \approx \sqrt{8E_J E_C} - E_C \tag{1.17}$$

So if changes on Qubit frequency value is needed, then it could be done by varying those two energies. This modification is applied either by a gate voltage V_g or bias external flux ϕ_e or even the two together. Both of them are crucial in determining the supercurrent that flows through the junction.

$$E(\varphi) = -E_J \cos(\varphi) \tag{1.18}$$

where φ is the phase difference across the junction.

$$\varphi = \frac{2\pi\Phi_{\text{ext}}}{\Phi_0} \tag{1.19}$$

Where:

- φ is the phase difference across the Josephson junction.
- Φ_{ext} is the external magnetic flux applied to the junction (measured in Webers, Wb).
- $\Phi_0 = \frac{h}{2e}$ is the magnetic flux quantum, where h is Planck's constant and e is the elementary charge.

The phase difference φ is proportional to the external flux Φ_{ext} through the junction. The constant of proportionality is $\frac{2\pi}{\Phi_0}$, which accounts for the quantization of flux in superconducting circuits. The magnetic flux quantum Φ_0 represents the smallest possible amount of flux that can be threaded through a superconducting loop, and this quantization plays a key role in the dynamics of the Josephson junction.

$$E_{\text{gate}} = 2en_g V_g \tag{1.20}$$

The second importance is that the ratio between E_c and E_j determines the type of superconducting Qubit, as it is explained next.

Superconducting Qubit Categories

The Qubit is a two-level system. In superconducting Quantum computers, it is realized by many designs that necessarily consist of one Josephson junction at least, exhibit the Josephson effects mentioned earlier. Yet, those many designs can be categorized into two types. The first is Charge Qubits and the second is Phase Qubits.

Which are different based on the characteristics of the Junction and the superconducting island-superconducting plates. For *charge Qubits*, The phase between the two superconducting wave functions is so little that not so many cooper pairs tunnel through the junction. As a result, the charge accumulates on the island, leading to a ratio $E_j/E_c < 1$. On the other hand. *Phase Qubit's* quantum states have different flux, in other words, the phase across the junction is unlike, and there will be gradient flow of cooper pair tunneling from one island to the other. In such a case the coupling junction energy E_j is larger than the charging energy E_c, so $E_j/E_c > 1$.

A Transmon Qubit is the type used in the architecture proposed in this paper. Its design is derived from the charge superconducting Qubit, such that its advancement contributes to solving one of the charge Qubti- cooper pair box- problems. Which is the Qubit's sensitivity to external charge; external voltage or the surrounding environment can significantly alter the Qubit's energy levels,

Circuit of Transmon Qubit This type is achieved by connecting a parallel Capacitor as shown in Fig1.1. Such a design makes charge insensitive Qubit design, while preserving adequate anharmonicity. Derived from cooper pair box [7]

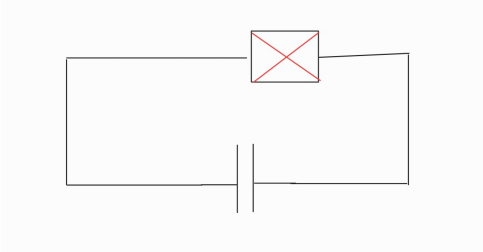

Figure 1.1: Transmon circuit schema. Josephson junction and parallel capacitor.

Realization of Two-level States ground state and excited state of the Transmon superconducting Qubit's are realized as follows.

In *the ground state*, a supercurrent passes through the Josephson junction due to the phase difference across its superconducting electrodes. Despite this current flow, the qubit remains in its lowest energy level without any spontaneous transitions to higher states. In this state, the qubit is energetically stable, and although its energy levels are defined, it does not exhibit transitions between them unless energy is externally supplied.

In comparison *the excited state*, energy is typically introduced to the system via microwave radiation, which causes the qubit to transition to a higher energy state. In this state, the qubit acquires a well-defined transition frequency—representing the energy difference between the ground and excited states. This frequency is fundamental to quantum operations, as it enables the qubit to oscillate between states and interact with other qubits or external electromagnetic fields.

While a supercurrent flows through the Josephson junction in both ground and excited states, the critical distinction lies in the system's behavior. The ground state is stable and non-oscillatory, while the excited state has a defined frequency associated with state transitions. This oscillation, or qubit frequency, is essential for enabling interactions such as quantum gate operations and coupling to other Qubits.

Single Qubit Operations and measurements

In General and similar to input output theory, a single Qubit gate is the process of imposing a sequence of excitations on the Qubit. And measurement is the process of getting a useful output of the those operations by readout the final quantum state of the Qubit.

For an engineered superconducting Qubits, the previous two processes are lightmatter interactions, which can be outlined in three architecture components.**A driver, Qubit, and a sensor.**

A driver is a microwave pulse that is regulated to have a signal frequency as the Qubit frequency to be able to excite it from its stable state to an excited state, where now it can be in multiple states at simultaneously.

On the other hand, reading out using a sensor usually incorporates two main parts. A comparator for checking the analog signal resulting from the flux or the charge in the loop which reflects the computational basis of the Qubit. In addition, an amplifier so that the state can be interpreted classically. More accurately, the electric or magnetic dipole moments are detected using a SQUID magnetometer, or a high sensitive electrometer like, (SFQ electronics)

Qubit-Read resonator and Qubit- Microwave Driver resonator handled according to *Jaynes Cumming model* [1]

The Hamiltonian of the Jaynes-Cummings model, which describes the interaction between a two-level system (qubit) and a single-mode electromagnetic field, is given by:

$$H_{\text{JC}} = \frac{\hbar}{2}\omega_0\sigma_z + \hbar g(\sigma_+ a + \sigma_- a^\dagger) \tag{1.21}$$

Here:

- ω_0 is the natural frequency of the two-level system (the qubit),
- σ_z is the Pauli z operator for the qubit, representing the energy splitting between the ground and excited states,
- g is the coupling constant between the qubit and the field mode,
- σ_+ and σ_- are the raising and lowering operators for the qubit, responsible for exciting and de-exciting the qubit between its ground and excited states, respectively,
- a and $a^\dagger$ are the annihilation and creation operators for the electromagnetic field mode.

This model describes the qubit-field interaction when the system is not driven by an external field. The qubit interacts with the electromagnetic field mode, and the energy exchange between them occurs via the coupling constant g.

When the Qubit is subject to an external time-dependent microwave drive, which can manipulate the Qubit's state. This drive adds an additional term to the Hamiltonian, modifying the Qubit's evolution. The time-dependent Hamiltonian for the system under a microwave drive can be written as:

$$H(t) = \frac{\hbar}{2}\omega\sigma_z + \hbar\Omega_0\cos(\omega_d t - \phi)\sigma_x \tag{1.22}$$

Where:

- ω is the qubit's frequency (the energy splitting between the ground and excited states),
- Ω_0 is the amplitude of the microwave drive (the Rabi frequency),
- ω_d is the frequency of the microwave drive,
- ϕ is the phase of the microwave drive,
- σ_x is the Pauli-x operator for the qubit.

This term, $\Omega_0\cos(\omega_d t - \phi)\sigma_x$, represents the interaction between the qubit and the time-dependent microwave drive. It introduces an oscillating component that can cause transitions between the ground and excited states of the qubit. The drive is typically chosen to be resonant or near-resonant with the qubit's natural frequency to manipulate the qubit's state efficiently.

To simplify the time-dependent behavior of the drive, we often move to the rotating frame, which eliminates the oscillating terms. This is done by applying a unitary transformation to the Hamiltonian. The resulting Hamiltonian in the rotating frame is:

$$H_{\text{rot}} = \frac{\hbar}{2}(\omega - \omega_d)\sigma_z + \hbar\Omega_0\left(\cos\phi\,\sigma_x + \sin\phi\,\sigma_y\right) \tag{1.23}$$

In this frame:

- The term $\frac{\hbar}{2}(\omega - \omega_d)\sigma_z$ describes the detuning between the qubit's natural frequency ω and the drive frequency ω_d,
- The term $\Omega_0 (\cos\phi\,\sigma_x + \sin\phi\,\sigma_y)$ describes the interaction between the qubit and the microwave field, now simplified to time-independent components along the x- and y-axes, with the phase ϕ dictating the relative weighting of the two components.

This transformation simplifies the problem by reducing the time dependence of the interaction, making the evolution of the qubit under the drive easier to analyze.

Superconducting Qubit-Qubit Coupling

Establishing connections between Qubits is a critical stage in designing the superconducting chip. This is to ensure that the chip has large enough information storage to make it useful. These connections are just channels for energy interchange, so there are so many physical types to realize such connections. To choose such interconnecting properly, one should consider the type of Qubits to be interconnected because one physical joint can work between charge Qubits but perform weak coupling between phase Qubits.

Tunable coupler

Coupling can be classified as fixed and tunable. The fixed coupling has a constant coupling strength in the direct energy exchange regime. While the tunable coupler has the ability to have real-time control over this strength.

Fixed couplers are implemented using passive elements like an inductor or a capacitor like the one shown in the Figure below.

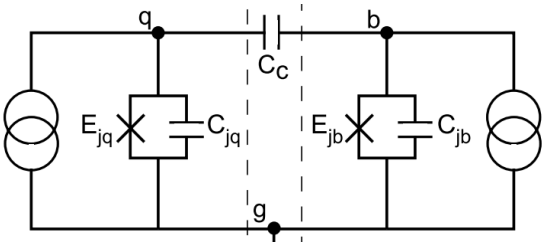

Figure 1.2: Fixed coupling. Capacitive coupling.[3]

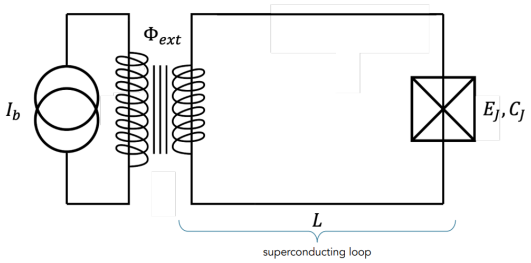

Figure 1.3: Fixed coupling, inductive coupling

Several architectures assemble permanent coupling between Qubits. However, the general operating mechanism for those fixed couples depends on the Qubit intrinsic properties specifically what is called **Plasma frequency.** Which refers to the natural oscillation frequency of the charge carriers impacting the behavior of the system in response to high-frequency signals.

For instance, one example of capacitive coupling [13] used to connect current biased Qubit the plasma frequency has the form

$$\omega_{\text{plasma}} = \sqrt{\frac{2\pi I_c}{\Phi_0 C_j}} \left(1 - \left(\frac{I}{I_c}\right)^2\right)^{1/4}$$

The inherent dependence on the plasma frequency of the Qubit imposes and amplifies limitations. For instance, frequency crowding, and cross talk.

In contrast, tunable couples are independent of the plasma frequency by their additional degree of freedom. Which reduced demand on certain frequency by so many Qubits.

Two Qubits gates

The physical connection between superconducting Qubits is not enough to mimic the electrons in an atom. One important Quantum mechanical property should be imitated, that is Entanglement. Which is done by conducting operations on the coupler Qubits - two Qubit gates.

The famous gates that are implemented in the abstract quantum languages are CNOT, SWAP, and CZ gates. Each one of them has a matrix representation that specify what happens to two Qubits undergoing them. For example, CNOT gate applied on a two Qubit would have a 2 by 2 matrix of the form.

$$\text{CNOT} = \begin{pmatrix} 1 & 0 & 0 & 0 \\ 0 & 1 & 0 & 0 \\ 0 & 0 & 0 & 1 \\ 0 & 0 & 1 & 0 \end{pmatrix}$$

and it can be deduced how this flips the target Qubit state if the control Qubit is the basis |1>. This is important in creating Entanglement between the two Qubits. However, experimentally, it is not an easy task to exactly flip the phase or exactly translate the Qubit to the theoretical final state underlined by the gate matrix. The closer the experimental result to theoretical predicted result, then the gate operation is said to have high fidelity.

Different gates fidelity are achieved based on the experimental method used. Such as cross resonance[5], frequency tuning gate [6], and parametric gate [14]. The major difference is how the microwave pulse is optimized in amplitude and frequency to approach the aim population and phase accumulation between states.

Advantage of Superconducting Qubits can be summarized as follows

- *Extensive design options*. As highlighted previously, there are several possible architectures for superconducting Qubit circuits. Not only this, but also the ability to adjust the values of the inductance, capacitance, and the nonlinear Josephson junction. Making this technology adaptable to different applications.
- *Convenient manipulations*. Many of the commercial classical electronics can be used for Qubit state readout, and control.
- *Scalability*. The overlapping process with the conventional silicon-based fabrication, and how it's built on existing tools elevate the chances of scaling up the devices.

Challenges of Designing superconducting Qubits

Qubit life-time

1.2.4 Lumped-Oscillator Model

Lumped models are well-established in classical circuit theory, used to manage distributed effects in components such as transmission lines by approximating them as discrete elements. IBM's adaptation of the Lumped Oscillator Model (LOM) in Qiskit Metal leverages this approach for quantum circuits, offering an efficient computational method to derive the system Hamiltonian by reducing the degrees of freedom, thus enabling faster simulation of superconducting circuit designs.

Network and Graph theory Network graph theory is used to analyze electrical circuits. And it has the following advantages over other methods

- Graph Representation. Components of the circuit are represented as nodes, and the connections between them are edges.
- Visualization. Makes complex circuits easier to understand by visualizing interconnections and relationships between components.
- Systematic Approach. Allows for structured application of Kirchhoff's Voltage and Current Laws (KVL and KCL) to derive the equations governing the system.
- Matrix Methods: Admittance or impedance matrices can be used to represent the circuit, allowing for efficient matrix operations to solve the system.

The building blocks to translate an electrical circuit into its corresponding graph are as follows. To begin with, for a graph G a *loop* is a sub-graph G_i. Each subgraph consists of a *Branch* B_i which corresponds to a two-ports element. Each port is between two elements that is a *Node* N_i. So the branch connects two nodes. A *Tree* T_i is a group of branches linking all nodes but containing no loop. As a result, there are two types of branches, ones that are in the tree and others that are not part of the tree which are called *chords*, each chord is associated with a distinct loop that is formed by adding the chord to the tree.

As a result, we can account for the total number of nodes N and branches B in a graph, let the number of disjoint-don't share a node- subgraphs be denoted by P. Then $\sum_{i=1}^{P} N_i = N$ and $\sum_{i=1}^{P} B_i = B$. One more constituent of a graph is a *Cutset* which is a set of the fewest branches that, when removed, partition the graph into two distinct subgraphs.

The LOM method harnesses the network graph theory to set up a partition protocol to map the distributed effects of the Quantum circuit into discrete and isolated effects. Where it follows the guidelines for cutsets and loop to Enable the execution of Kirchhoff's laws to capture the current an voltage corresponding to the charge and the flux as derived in section 1.2.2.

When the distributed effects of a system are taken into account, the capacitance and inductance cannot be directly expressed as the sum of the capacitance or inductance matrices of individual elements. However, when these effects are simplified using the Lumped Oscillator Model (LOM), the following approximations become valid:

$$C_n = \sum_{n=0}^{N} C_{n;\text{cell}} \tag{1.24}$$

$$L_n^{-1} = \sum_{n=0}^{N} L_{n;\text{cell}}^{-1} \tag{1.25}$$

The inductive and capacitive coupling on the nodes imposes coupling constraints on the complex system. Three dressing adjustments are applied to this method to address these boundaries. The first is capacitive dressing, the second is inductive dressing, and finally the inverse of the capacitance. As described in Chapter 2.

Experimental Agreement.

To demonstrate the feasibility of simulating quantum processors by following the LOM protocol, a team from IBM [10] compared the results of simulations to the experimentally realized results of a superconducting chip.

The processor in their case study contained coplanar waveguides for coupling and reading out connection. And it was regulated by charge lines. In the laboratory, readout photon number and dispersive shift χ were estimated by conventional spectroscopic and time-resolved methods.

On the other hand, applying LOM started by extracting the Maxwell capacitance matrix of the geometrical layout using Ansys Q3D extractor, then dressing the Matrix and accounting for the renormalization.

The dispersive shift between Qubits and cavities χ_{qr} was analyzed. 19% agreement was achieved between LOM prediction and experimental results. To bridge the gap and add improvements, they believe variation should be made in terms of parameters like L_j and impedance Z_0 identification throughout the EM radiation because the geometry of the device has exact, clear effects so their uncertainty is low. On top of that, they suggest that the protocol should take into consideration a more detailed description of the distributed effects.

Chapter 2

Methodology

2.1 Target analysis

The LOM protocol will be applied on the tunable coupler circuit motivated from [2]. Shown in the figure below.

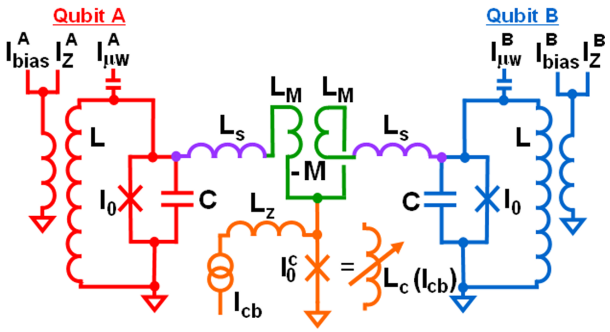

Figure 2.1: Four unit module tunable coupler connecting two phase Qubits.

Qubit-qubit interactions across different platforms are facilitated by coupler circuits that are inductively linked to the Qubits. Numerous theoretical studies have been conducted on these circuits such as in [9],[11, p. 8] However, inductive coupling wouldn't be useful with certain types of Qubits, such as charge Qubits; it will lead to weak coupling because the charge Qubits have almost a fixed phase across their junction, so one should consider the type of Qubits to engineer a well-behaved coupler.

The class of superconducting Transmon Qubits that are coupled here are phase Qubits. This kind is sensitive to the smallest flux variations, this fact is employed in the design of the structure of the Tunable coupler in Fig1.2. Such that the main three components are an autotransformer, a Josephson junction, and a current bias to control the junction. On the other hand, the other two series inductors scale down the coupling effects.

The inductive element is a must in this case, that is because the coupling mechanism of the phase Qubits is flux-based. Yet, a simple inductor will not serve the controlled coupling that we aim for. Instead, an autotransformer is used as a flux-sharing mechanism to support the coupling. Where it facilitates coupling via its third node mid-the-windings. Moreover, the compact design of the autotransformer allows for energy retention for a longer time, as a result, reduces the quantum coherence time of the circuit.

The tunability is achieved through nonlinear Josephson elements which control the coupling strength g between the two Qubits. Because the coupling is flux-based then the variation in the phase across the junction will lead to fluctuation in flux in the autotransformer, as a result, the coupling will be either increased or decreased.

The expected added value of this architecture is its speed. Employing the high sensitivity of Josephson junction to the current passing through it when controlling the biased current. This

results in not only a quick response of the coupling strength between the Qubits but also a fine-tuning ability to small differences. Lastly, and more importantly, these two advantages should lead to more isolated Qubits when the coupling strength is at a minimum, in other words, it will reduce the cross-talk between Qubits. In the following, the low cross-talk property will be investigate further.

Per the LOM described in Chapter 1. The following will be applied to analyze the tunable structure

- LOM Partitions. choose the loops in the circuit and partition the circuit accordingly, using the Cutset concept. Sometimes, only a segment of a complex circuit so instead of relying on loops to partition the circuit, the division occurs based on the energy distribution; its Hamiltonian H_n has a well-known structure and can be diagonalized. Most importantly, can be expressed in Harmonic-Oscillator Basis.
- Simulates each cell
- Map the composite system into subsystem building blocks by finding Lagrangian
- Legendre transformation on L to find the Hamiltonian
- Apply dressing to the system to eliminate constraints by transformation. Which will reduce the system from N to N-r degrees of freedom. One is to dress the Capacitance matrix: adjust and modify its value and the other of the inverse of the inductance matrix.

2.2 Mathematical Framework

I will begin by deriving a general description of the energy eigenvalues of a system consisting of two coupled quantum systems. Their respective energies give the Hamiltonian of the uncoupled systems, and the coupling introduces a perturbation term.

Hamiltonian

Consider two uncoupled quantum systems with energy levels E_1 and E_2, and a coupling term represented by g. The Hamiltonian of the uncoupled systems is:

$$H_0 = H_1 + H_2$$

where H_1 and H_2 are the Hamiltonians of the two individual systems. When the two systems interact, we include a coupling term g, and the total Hamiltonian of the coupled system becomes:

$$H = \begin{pmatrix} E_1 & g \\ g & E_2 \end{pmatrix}$$

Here, g represents the coupling strength between the two systems, and E_1, E_2 are the energy levels of the individual systems.

Diagonalizing the Hamiltonian

To find the energy eigenvalues of this system, we solve for the eigenvalues of the Hamiltonian matrix H. The eigenvalues λ are found by solving the characteristic equation:

$$\det(H - \lambda I) = 0$$

where I is the identity matrix and λ is the eigenvalue. This gives:

$$\det \begin{pmatrix} E_1 - \lambda & g \\ g & E_2 - \lambda \end{pmatrix} = 0$$

Expanding the determinant:

$$(E_1 - \lambda)(E_2 - \lambda) - g^2 = 0$$

This simplifies to the quadratic equation:

$$\lambda^2 - (E_1 + E_2)\lambda + (E_1 E_2 - g^2) = 0$$

Solving the Quadratic Equation

We solve the quadratic equation for λ using the quadratic formula:

$$\lambda_\pm = \frac{(E_1 + E_2) \pm \sqrt{(E_1 + E_2)^2 - 4(E_1 E_2 - g^2)}}{2}$$

Simplifying the discriminant:

$$\lambda_\pm = \frac{E_1 + E_2}{2} \pm \sqrt{\left(\frac{E_1 - E_2}{2}\right)^2 + g^2}$$

Thus, the energy eigenvalues of the coupled system are:

$$\lambda_\pm = \frac{E_1 + E_2}{2} \pm \sqrt{\left(\frac{E_1 - E_2}{2}\right)^2 + g^2}$$

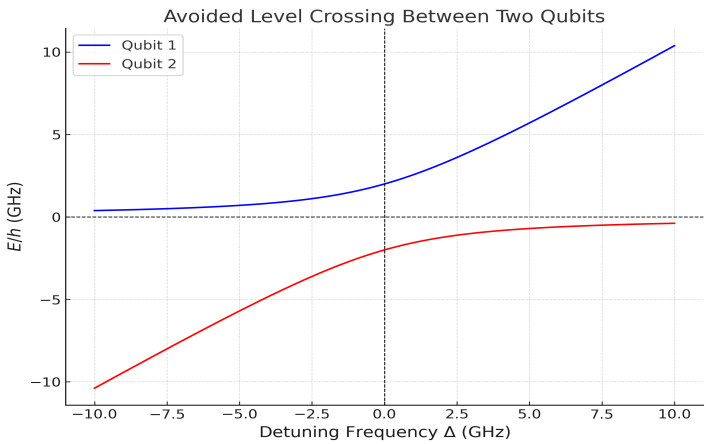

Figure 2.2: Standard Avoided level crossing graph

The coupling strength g formula differs based on the physical coupling mechanism. Throughout this chapter, g will be derived for the tunable coupled system used in connecting the two phase_Qubits

According to [10] the Hamiltonian of the composite system after degrees of freedom reduction, and individual cell simulation, should have the following form.

$$H_{\text{full}} = H_0 + \sum_{n=1}^{K_1} H_n + \sum_{n=0}^{K} \sum_{m=n+1}^{K} H_{nm} \tag{2.1}$$

$$H_{nm} = \frac{Q_n Q_m}{C_{\text{nm}}^{eff}} + \frac{\phi_n \phi_m}{L_{\text{nm}}^{eff}} \tag{2.2}$$

For N cells in the composite system, rewrite Eq1.18 and Eq1.19 in their matrix form.

$$C_n = \sum_{n=0}^{N} \begin{bmatrix} c_{11} & c_{12} & \dots \\ c_{21} & c_{22} & \dots \\ \vdots & \vdots & \ddots \end{bmatrix} \tag{2.3}$$

$$L_{n,\text{cell}}^{-1} = \begin{bmatrix} l_{11} & l_{12} & \dots \\ l_{21} & l_{22} & \dots \\ \vdots & \vdots & \ddots \end{bmatrix} \tag{2.4}$$

The Lagrangian of the multicomponent system is as follows. Where ϕ_n is the node_to_datum flux column. and the C_n and L_n^{-1} are the capacitance and inverse inductance matrices of the composite system respectively.

$$L = T - V \tag{2.5}$$

$$Q = C_n \dot{\phi}_n \tag{2.6}$$

$$T = \frac{Q^2}{2C_n} \tag{2.7}$$

$$V_{\text{inductors}} = \frac{\phi_n^2}{2L_n} \tag{2.8}$$

$$V_{\text{non-linear}} = \sum_{j=1}^{J} \epsilon_{j,nl} \tag{2.9}$$

$$\epsilon_{j,nl} = \epsilon_{j,\text{lin}} - \frac{1}{2} L_j^{-1} \phi_j^2 \tag{2.10}$$

$$L = \frac{C_n \dot{\phi}_n^2}{2} - \left(\frac{\phi_n^2}{2L_n} + \sum_{j=1}^{J} \left(\epsilon_{j,\text{nl}} \right) \right) \tag{2.11}$$

The interaction between components is reciprocal. As a result, capacitance and inverse inductance matrices are symmetric, $Q^T = Q$ and $\Phi^T = \Phi$. Thus matrix representation is used for convenience.

$$L_n(\dot{\phi}_n, \phi_n) = \frac{1}{2} \dot{\phi}_n^T C_n \dot{\phi}_n - \frac{1}{2} \phi_n^T L_n^{-1} \phi_n - \sum_{j=1}^{J} \epsilon_n^{\text{nl}}(\phi_j) \tag{2.12}$$

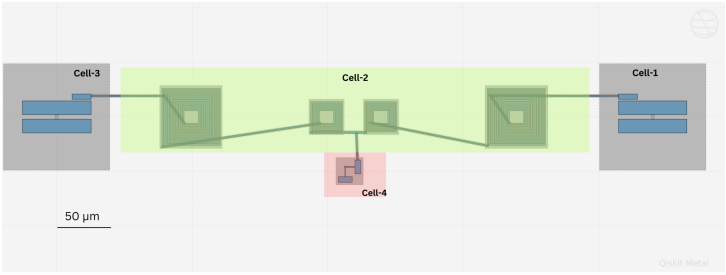

Figure 2.3: Partition the composite system according to network graph theory into cells

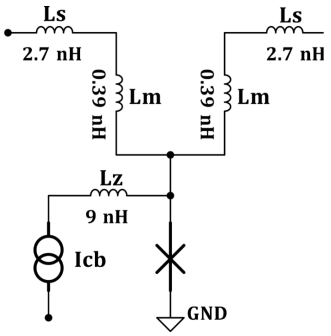

Figure 2.4: Circuit Schema of the tunable coupler, corresponding to cell 2, and 4

$$\hat{H}_n = \frac{1}{2}\hat{Q}_n^T C_n^{-1}\hat{Q}_n + \frac{1}{2}\hat{\Phi}_n^T L_n^{-1}\hat{\Phi}_n + \sum_{j=1}^{J}\epsilon_n^{\text{nl}}(\phi_j) \tag{2.13}$$

Let us define the flux of the j-th dipole as

$$\Phi_j = \Phi_{n2} - \Phi_{n1}$$

and the external flux, which is caused by the changing inductance of L_{m1} and L_{m2}, by ϕ_{ext}. Then each Hamiltonian cell of Figure 2.3 can be found to be as follows, similar to [12] with capacitance and inductance being dressed.

Cell_1

The first cell is a phase Qubit that consists of the junction, capacitor ,and the coplanar waveguide subsystem.

$$\begin{aligned}\hat{H}_{\text{cell1}} = &\frac{Q_1^2}{2C_1\Phi_0} - E_{J1}\cos(\Phi_1) + \frac{\Phi_0^2}{2L_1}(\Phi_1 - \Phi_{\text{ext},1})^2 \\ &+ \left(\frac{M}{L_{m1}L_{m2}}\right)\Phi_0^2\left((\Phi_1 - \Phi_4 - \Phi_{\text{ext},m1})^2 \cdot (\Phi_3 - \Phi_4 - \Phi_{\text{ext},m2})^2\right)\end{aligned} \tag{2.14}$$

Cell_3

The second Qubit would have a similar Hamiltonian with different capacitance and flux-node to datum.

$$\begin{aligned}\hat{H}_{\text{cell3}} = &\frac{Q_3^2}{2C_3\Phi_0} - E_{J3}\cos(\Phi_3) + \frac{\Phi_0^2}{2L_3}(\Phi_3 - \Phi_{\text{ext},3})^2 \\ &+ \left(\frac{M}{L_{m1}L_{m2}}\right)\Phi_0^2\left((\Phi_1 - \Phi_4 - \Phi_{\text{ext},m1})^2 \cdot (\Phi_3 - \Phi_4 - \Phi_{\text{ext},m2})^2\right)\end{aligned} \tag{2.15}$$

Cell_4

This cell describes the Josephson junction used to control the coupler via a biased current.

$$\hat{H}_{\text{cell4}} = E_{J4}\cos(\Phi_3) - I_B \cdot \Phi_0\Phi_4 \tag{2.16}$$

Cell_3

The set of inductors that contribute to tuning the coupling should behave as follows.

$$\begin{aligned}\hat{H}_{\text{cell2}} = \frac{\Phi_0^2}{2L_{m1}}(\Phi_1 - \Phi_4 - \Phi_{\text{ext},m1})^2 + \frac{\Phi_0^2}{2L_{m2}}(\Phi_2 - \Phi_4 - \Phi_{\text{ext},m2})^2 \\ + \frac{Q_1Q_2}{C_1C_2}\Phi_0^2\end{aligned} \tag{2.17}$$

From all the parameters that can be extracted from the Hamiltonian. This study focuses on the coupling strength between the phase Qubits. Hence, the characteristic equation will be solved only for the coupling Hamiltonian of the circuit, which can extracted from the cells to be

$$\hat{H}_c = \frac{Q_1Q_2}{(C_1C_2\Phi_0)^2} + \Phi_0^2\left[\left(\frac{M}{L_{m1}L_{m2}}\Phi_1\Phi_2\right) - \frac{1+\frac{M}{L_{m1}}\Phi_1\Phi_4}{L_{m2}} - \frac{1+\frac{M}{L_{m2}}\Phi_2\Phi_4}{L_{m1}}\right] \tag{2.18}$$

The Capacitance matrix of the Qubits tunable coupler and the inverse inductance matrix will have the following form.

$$C_{\text{global}} = \begin{pmatrix} C_{1,\text{cell}} & C_{12}^{\text{eff}} & C_{13}^{\text{eff}} & C_{14}^{\text{eff}} \\ C_{21}^{\text{eff}} & C_{2,\text{cell}} & C_{23}^{\text{eff}} & C_{24}^{\text{eff}} \\ C_{31}^{\text{eff}} & C_{32}^{\text{eff}} & C_{3,\text{cell}} & C_{34}^{\text{eff}} \\ C_{41}^{\text{eff}} & C_{42}^{\text{eff}} & C_{43}^{\text{eff}} & C_{4,\text{cell}} \end{pmatrix} \tag{2.19}$$

Where each capacitance on the diagonal is a block matrix that corresponds to the capacitance of individual n_cells containing its node's capacitance and inner system capacitance. From the figure, we see that C_1 and C_2 have 2 nodes, so they are 2×2, and C_3 which is the inductors network has 9 nodes, so it is a 9×9 matrix. Lastly, the Josephson junction cell has 3 nodes, 3×3 matrix.

Similarly, the 4-cell system has the following inverse inductance matrix.

$$L_{\text{global}}^{-1} = \begin{pmatrix} L_{1,\text{cell}}^{-1} & L_{12}^{\text{eff}} & L_{13}^{\text{eff}} & L_{14}^{\text{eff}} \\ L_{21}^{\text{eff}} & L_{2,\text{cell}}^{-1} & L_{23}^{\text{eff}} & L_{24}^{\text{eff}} \\ L_{31}^{\text{eff}} & L_{32}^{\text{eff}} & L_{3,\text{cell}}^{-1} & L_{34}^{\text{eff}} \\ L_{41}^{\text{eff}} & L_{42}^{\text{eff}} & L_{43}^{\text{eff}} & L_{4,\text{cell}}^{-1} \end{pmatrix} \tag{2.20}$$

In comparison, the off-diagonal block matrices correspond to the capacitive coupling between cells.

2.3 Computational Framework

In this section, three main aspects will be discussed. The software used in the analysis, general guide of the process, and the layout of each component in the module tunable circuit. The detailed code can be found on Sarah's Dweik GitHub

Qiskit Metal

It is an open-source software from IBM, specializing in designing superconducting Quantum chips. Surpassing other layout programs like KQCircuit by its ability to encode the layouts and activate elements to be able to connect them directly with simulations. Thus, you don't just visualize your chip, but also test your dimension choice and arrangement of the elements, check for parasitic effects and extract parameters to evaluate metrics of the architecture used. A general outline of the workflow of the software is shown below.

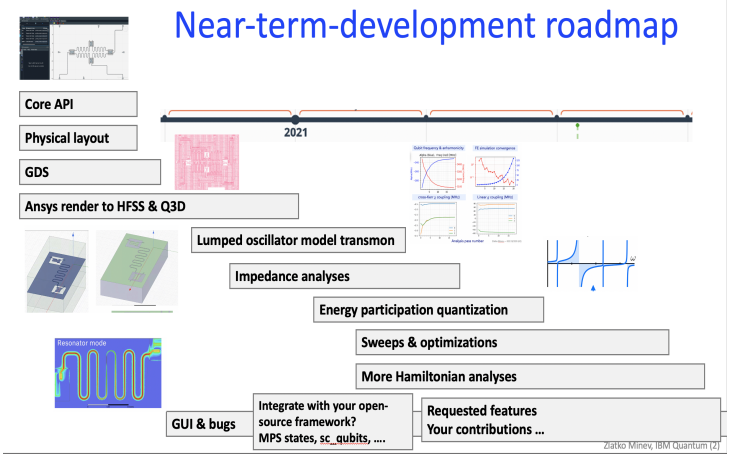

Figure 2.5: Qiskit Metal Bird eye overview. https://qiskit-community.github.io/qiskit-metal/workflow.html

The operation flow can be briefly described beginning by creating geometric, and most likely that your geometry will belong to one of the parent classes in Qiskit Metal are *BaseQubit*, *QComponents*, and *QDesign*. Then the geometry should be converted to geometry to be activated, to route the component, pins should be added to the structure. Dimensions can be edited from the options dictionary of the component. The main imports needed for the tunable coupler design are shown in code snippet below.

```
#imports
from qiskit_metal import Dict, designs, MetalGUI
from qiskit_metal.qlibrary.sample_shapes.n_square_spiral import NSquareSpiral
from qiskit_metal.qlibrary.qubits.transmon_pocket import TransmonPocket
from qiskit_metal.qlibrary.qubits.JJ_Manhattan import jj_manhattan
from qiskit_metal.qlibrary.tlines.straight_path import RouteStraight
from qiskit_metal.qlibrary.terminations.open_to_ground import OpenToGround
import numpy as np
from pocket import Pocket
```

Listing 2.1: Design imports in Qiskit Metal

Figures 2.6 to 2.9 are from the Qiskit Metal, graphical user interface, GUI. The dimensions of the connection on the chip are

```
design.variables['cpw_width'] = '0.5um'
design.variables['cpw_gap'] = '0.3um'
```

Listing 2.2: Qiskit Metal some dimensions instructions

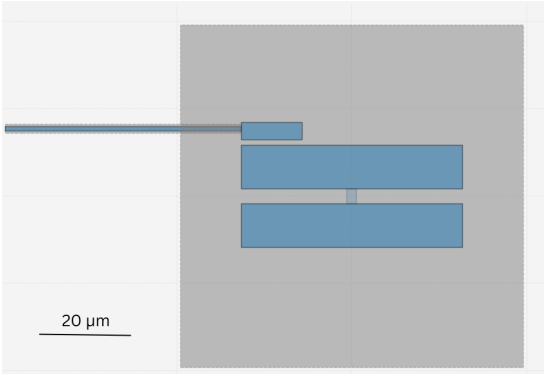

Figure 2.6: Transmon Qubit layout on Qiskit Metal GUI

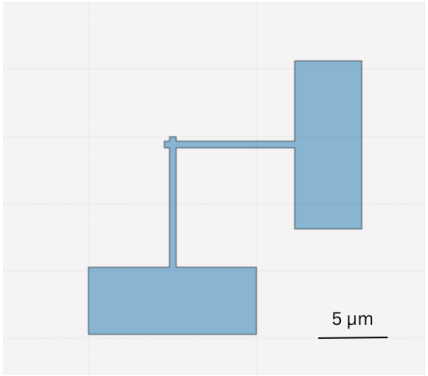

Figure 2.7: Manhattan Josephson junction layout on the GUI

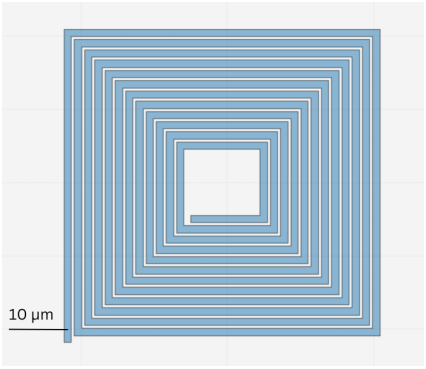

Figure 2.8: Series planer square inductor with value 2.7 nH

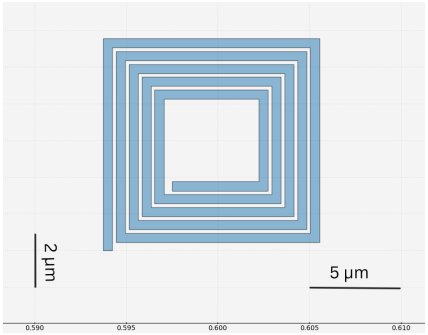

Figure 2.9: Autotransformer planer square inductor with value 0.39 nH

The tunable architecture implemented in this work adds value to Qiskit Metal, which includes a built-in capacitive tunable coupling architecture inspired by [16]. However, as shown in Figure 2.3, the architecture in this work is based on inductive tunable coupling.

Ansys Desktop Electronics

The second software that comes in handy when attempting to study and analyze this architecture is Ansys. Which is a leading engineering simulation software used to model, analyze, and solve complex problems across various industries. It provides a wide range of tools for simulating physical phenomena such as structural mechanics, fluid dynamics, electromagnetics, and thermal analysis. By utilizing powerful numerical methods like the Finite Element Method (FEM) and Finite Volume Method (FVM), Ansys enables engineers and researchers to optimize designs, predict performance, and reduce the need for physical prototyping. Its applications span aerospace, automotive, electronics, energy, and more, making it a critical tool for innovation and problem-solving.

Ansys was used for several purposes across the work. As expected it was employed for 3D conversion and mesh generation of the design. In addition, the maxwell solver in Ansys was utilized to extract and estimate an empirical formula for the self-inductance relation of the spiral square inductor used in the superconducting quantum chip layout in Qiskit Metal.

Mesh generation plays a vital role in the structural analysis. By dividing a complex geometry into smaller, discrete elements. During a simulation, quantities like electric or magnetic fields are calculated at each mesh element, helping to model the system's behavior in response to internal or external forces. The mesh turns a continuous domain into a more manageable form, making it possible to simulate and understand real-world phenomena that would otherwise be too complex to solve analytically.

Chapter 3

Results and Discussion

3.1 Device Geometry

The first geometric parameters to examine are the tunneling energy, denoted by E_j, and the charging energy, E_c, which represents the energy required to add one more Cooper pair. These intrinsic properties are determined by the specific dimensions and physical configuration of the layout. Accurately identifying the values of E_j and E_c is crucial for two main reasons.

First, they are essential for calculating the qubit frequencies, which allows us to later observe any changes that may occur due to coupling effects. Second, determining the critical current is necessary to ensure that the quantum behavior is maintained. In particular, the current should not exceed the critical value during electromagnetic simulations, as surpassing this threshold could disrupt the desired quantum properties.

By focusing on these parameters, we can better understand the system's behavior and maintain proper conditions for quantum coherence. Bellow is a code snippets to extract such parameters, along with the data table.

```
c2.setup.junctions=Dict(Lj=12.31, Cj=2)
c2.setup.freq_readout = 5.0
c2.setup.freq_bus = []

c2.run_lom()
c2.lumped_oscillator_all
```

Listing 3.1: Extract main Qubits parameters E_j, E_c, f_q

Passes	f_Q **(GHz)**	E_C	E_J
1	5.848645	366.675723	13.273404
2	5.800484	360.198673	13.273404
3	5.728978	350.706154	13.273404
4	5.645726	339.839946	13.273404
5	5.574615	330.715418	13.273404
6	5.552051	327.850119	13.273404
7	5.522295	324.093652	13.273404
8	5.508895	322.410099	13.273404
9	5.492369	320.340887	13.273404

Table 3.1: Controlling Josephson junction parameters for different current biases.

3.2 Coupling Strength

Solving the coupling interaction Hamiltonian derived in chapter 2 assuming harmonic eigenfunction to find the formula of the coupling strength g.

$$\hat{H}\psi = E\psi$$

$$\hat{H}_c = \frac{Q_1 Q_2}{(C_1 C_2 \Phi_0)^2} + \Phi_0^2 \left[\frac{M\Phi_1\Phi_2}{L_{m1}L_{m2}} - \frac{1+\frac{M\Phi_1\Phi_4}{L_{m1}}}{L_{m2}} - \frac{1+\frac{M\Phi_2\Phi_4}{L_{m2}}}{L_{m1}} \right]$$

$$\psi_n(\Phi_1, \Phi_2, \Phi_4) = N_n \prod_i H_n \left(\sqrt{\frac{m\omega}{\hbar}} \Phi_i \right) e^{-\frac{m\omega\Phi_i^2}{2\hbar}}$$

where H_n is the Hermite polynomial, m is the mass, and ω is the angular frequency. Each flux Φ_1, Φ_2, Φ_4 behaves like a harmonic oscillator.

Then to be able to use harmonic oscillation wavefunction approximation, then one must linearize the potential and keep quadratic terms.

$$\hat{H}_c \approx \frac{Q_1 Q_2}{(C_1 C_2 \Phi_0)^2} + \frac{1}{2} \left(\alpha\Phi_1^2 + \beta\Phi_2^2 + \gamma\Phi_4^2 \right)$$

The approximation employed here is known as the rotating wave approximation (RWA), a commonly used technique in quantum mechanics and electrodynamics. It simplifies the analysis of systems where interactions occur between matter (such as atoms or qubits) and oscillating electromagnetic fields. The RWA assumes that terms oscillating at much higher frequencies than the system's characteristic frequency can be ignored. This allows the focus to remain on the slower-varying terms that have a meaningful impact on the system's behavior.

So the frequency splitting due to the symmetric and antisymmetric modes of qubit-qubit interaction-coupling strength g in Figure 2.2 of the avoided level crossing. is found to be

$$g = \frac{M - \frac{L_4}{1-\left(\frac{\omega_{qb}}{\omega_3}\right)^2}}{L_{m1}L_{m2}\omega_{qb}\sqrt{C_1 C_2}} + \frac{\omega_{qb}}{\sqrt{C_1 C_2}} \tag{3.1}$$

- M: Negative mutual inductance of the autotransformer, representing the magnetic coupling effect.
- L_4: Effective inductance of the coupling Josephson junction, tuned via the bias current I_B to enable adjustable coupling.
- ω_{qb}: Qubit frequency at zero detuning between the two qubits.
- ω_3: Resonant frequency of the coupler, determined by L_3 and C_3.
- L_{m1}, L_{m2}: Inductance of the autotransformer that connects the qubits to the coupler.
- C_1, C_2: Capacitance matrices associated with the two qubit cells.

3.3 Dispersive shift analysis

In circuit QED, the **dispersive shift** arises from the dependence of the Qubit's frequency on the state of the resonator. Fluctuations in the number of photons in the resonator, caused by residual microwave fields, result in a shift of the Qubit's intrinsic frequency. As a result, it can be thought of as a noise measurement scale. Detuning regimes reflect different dispersive shifts, where dispersive shift χ is maximum when the Qubits are directly exchanging energies when they are at resonance. On the other hand, this shift should be as minium as possible when the Qubits are detuned. And according to [8] it can be expressed as

$$\chi \approx \frac{g^2}{\Delta} \tag{3.2}$$

In this work, the dispersive shift between the two Qubits due to the existence of the tunable coupler is used as an indicator of having low or high crosstalk. when the Qubits are decoupled and the coupling strength is at minimum different

Applying the lumped elements approximation the capacitive effect between different nodes across the layout.

```
from qiskit_metal.analyses.quantization import LOManalysis
c2 = LOManalysis(design, "q3d")
q3d = c2.sim.renderer
q3d.start()
q3d.activate_ansys_design("TransmonResonator_q3d", 'capacitive')
q3d.render_design(['Q4','Q5','open1i','spiralm1','spiralm2','spiralS1','
    spiralS2','JJ2','cpw1','cpw2','cpw4','cpw5','cpw6','cpw7'], [])
q3d.analyze_setup("Setup")
c2.sim.capacitance_matrix, c2.sim.units = q3d.get_capacitance_matrix()
c2.sim.capacitance_all_passes, _ = q3d.get_capacitance_all_passes()
c2.sim.capacitance_matrix
```

Listing 3.2: Code snippet to extract capacitance matricies

Part 1: a_connector_pad_Q4 to n_spiral_spiralm1

	a_connector_pad_Q4	b_connector_pad_Q5	design_JJ2	ground_main_plane	n_spiral_spiralm1
a_connector_pad_Q4	0.000000	-0.000239	-0.000623	-6.645187	-0.001836
b_connector_pad_Q5	-0.000239	0.000000	-0.000365	-5.117250	-0.071335
design_JJ2	-0.000623	-0.000365	0.000000	-2.201198	-0.014763
ground_main_plane	-6.645187	-5.117250	-2.201198	0.000000	-12.447755
n_spiral_spiralm1	-0.001836	-0.071335	-0.014763	-12.447755	0.000000

Part 2: n_spiral_spiralm2 to pad_top_Q5

	n_spiral_spiralm2	pad_bot_Q4	pad_bot_Q5	pad_top_Q4	pad_top_Q5
n_spiral_spiralm2	0.000000	-0.001567	-0.000787	-0.001423	-0.005517
pad_bot_Q4	-0.001567	0.000000	-0.000156	-0.104701	-0.000209
pad_bot_Q5	-0.000787	-0.000156	0.000000	-0.000233	-0.861757
pad_top_Q4	-0.001423	-0.104701	-0.000233	0.000000	-0.000214
pad_top_Q5	-0.005517	-0.000209	-0.861757	-0.000214	0.000000

From the values of obtained in table 3.1 E_c, E_j. The average critical current was 34 mA. And from Ansys 3D analysis, the mutual inductance of the autotransformer is found to be 190 pH. Substituting found values in the coupling formula g. And then in Eq 3.2 for different current bias values. The following plot was obtained.

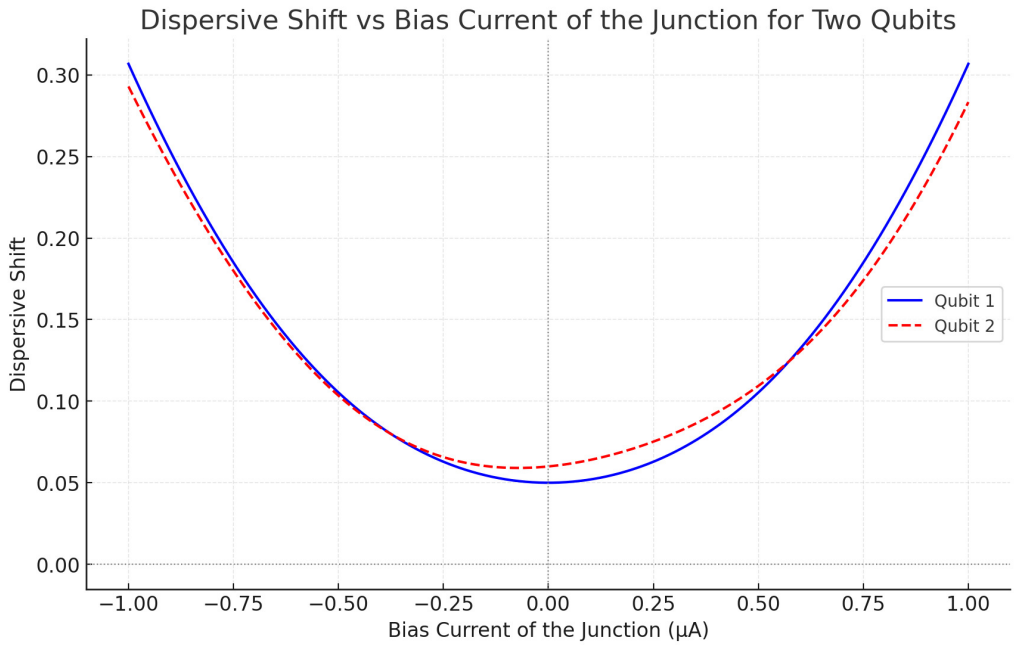

Figure 3.1: Dispersive shift Vs Tunable coupler bias current.

The simulation frequency is set to 5 GHz. When the bias current is zero, the tunable coupler is turned off, it is noted that the dispersive shift is = 0.05 MHz, which is quite low and corresponds to muted interaction between Qubit, in other words, they have low crosstalk as was expected.

3.4 Summary and Conclusion

Using the LOM in the analysis indeed was computationally efficient, such that time and space sources were relatively optimized.

Even though LOM protocol proved good approximation for validating the quality of isolation for this tunable coupler, however, there are other parameters to be investigated like the speed of the coupler to be able to generalize its efficiency and capacity.

The examined architecture is believed to have other advantages regarding single Qubit gate fidelity, where it has dynamics similar to real algorithm gate time. On top of that, the module should be able to couple elements despite the implemented topology, in other words, it extends beyond connecting near Qubits only. These features were not studied here, however, for future advances the LOM can be investigated more to see it can prove such properties.

3.5 References

Bibliography

[1] Adan Azem. Jaynes-cummings model, 1963.

[2] R. C. Bialczak, M. Ansmann, M. Hofheinz, M. Lenander, E. Lucero, M. Neeley, A. D. O'Connell, D. Sank, H. Wang, M. Weides, J. Wenner, T. Yamamoto, A. N. Cleland, and J. M. Martinis. Fast tunable coupler for superconducting qubits. *Physical Review Letters*, 106, 2 2011.

[3] Alexandre Blais, Alexander Maassen Van Den Brink, and Alexandre M Zagoskin. Tunable coupling of superconducting qubits, 2003.

[4] Alexandre Blais, Arne L. Grimsmo, S. M. Girvin, and Andreas Wallraff. Circuit quantum electrodynamics. *Reviews of Modern Physics*, 93, 5 2021.

[5] Jerry M. Chow, A. D. Corcoles, Jay M. Gambetta, Chad Rigetti, B. R. Johnson, John A. Smolin, J. R. Rozen, George A. Keefe, Mary B. Rothwell, Mark B. Ketchen, and M. Steffen. A simple all-microwave entangling gate for fixed-frequency superconducting qubits. 6 2011.

[6] L. Dicarlo, J. M. Chow, J. M. Gambetta, Lev S. Bishop, B. R. Johnson, D. I. Schuster, J. Majer, A. Blais, L. Frunzio, S. M. Girvin, and R. J. Schoelkopf. Demonstration of two-qubit algorithms with a superconducting quantum processor. *Nature*, 460:240–244, 7 2009.

[7] Jens Koch, Terri M Yu, Jay Gambetta, A A Houck, D I Schuster, J Majer, Alexandre Blais, M H Devoret, S M Girvin, and R J Schoelkopf. Charge insensitive qubit design derived from the cooper pair box, 2007.

[8] P. Krantz, M. Kjaergaard, F. Yan, T. P. Orlando, S. Gustavsson, and W. D. Oliver. A quantum engineer's guide to superconducting qubits. *Applied Physics Reviews*, 6, 6 2019.

[9] Yuriy Makhlin, Gerd Scho È, Alexander Shnirman, and C J V X X. Josephson-junction qubits with controlled couplings, 1999.

[10] Zlatko K. Minev, Thomas G. McConkey, Maika Takita, Antonio D. Corcoles, and Jay M. Gambetta. Circuit quantum electrodynamics (cqed) with modular quasi-lumped models. 3 2021.

[11] T P Orlando, J E Mooij, Lin Tian, Caspar H Van Der Wal, L Levitov, Seth Lloyd, and J J Mazo. A superconducting persistent current qubit, 11 2024.

[12] Ricardo A. Pinto, Alexander N. Korotkov, Michael R. Geller, Vitaly S. Shumeiko, and John M. Martinis. Analysis of a tuneable coupler for superconducting phase qubits. 6 2010.

[13] R. C. Ramos, F. W. Strauch, P. R. Johnson, A. J. Berkley, H. Xu, M. A. Gubrud, J. R. Anderson, C. J. Lobb, A. J. Dragt, and F. C. Wellstood. Capacitively coupled josephson junctions: A two-qubit system. In *IEEE Transactions on Applied Superconductivity*, volume 13, pages 994–997, 6 2003.

[14] Matthew Reagor, Christopher B Osborn, Nikolas Tezak, Alexa Staley, Guenevere Prawiroatmodjo, Michael Scheer, Nasser Alidoust, Eyob A Sete, Nicolas Didier, Marcus P Da Silva, Ezer Acala, Joel Angeles, Andrew Bestwick, Maxwell Block, Benjamin Bloom, Adam Bradley, Catvu Bui, Shane Caldwell, Lauren Capelluto, Rick Chilcott, Jeff Cordova, Genya Crossman, Michael Curtis, Saniya Deshpande, Tristan El Bouayadi, Daniel Girshovich, Sabrina Hong, Alex Hudson, Peter Karalekas, Kat Kuang, Michael Lenihan, Riccardo Manenti, Thomas Manning, Jayss Marshall, Yuvraj Mohan, William O'brien, Johannes Otterbach, Alexander Papageorge,

Jean-Philip Paquette, Michael Pelstring, Anthony Polloreno, Vijay Rawat, Colm A Ryan, Russ Renzas, Nick Rubin, Damon Russel, Michael Rust, Diego Scarabelli, Michael Selvanayagam, Rodney Sinclair, Robert Smith, Mark Suska, Ting-Wai To, Mehrnoosh Vahidpour, Nagesh Vodrahalli, Tyler Whyland, Kamal Yadav, William Zeng, and Chad T Rigetti. A p p l i e d s c i e n c e s a n d e n i g i n e e r i n g demonstration of universal parametric entangling gates on a multi-qubit lattice, 2018.

[15] Matthew Reagor, Wolfgang Pfaff, Christopher Axline, Reinier W. Heeres, Nissim Ofek, Katrina Sliwa, Eric Holland, Chen Wang, Jacob Blumoff, Kevin Chou, Michael J. Hatridge, Luigi Frunzio, Michel H. Devoret, Liang Jiang, and Robert J. Schoelkopf. A quantum memory with near-millisecond coherence in circuit qed. 8 2015.

[16] Youngkyu Sung, Leon Ding, Jochen Braumüller, Antti Vepsäläinen, Bharath Kannan, Morten Kjaergaard, Ami Greene, Gabriel O. Samach, Chris McNally, David Kim, Alexander Melville, Bethany M. Niedzielski, Mollie E. Schwartz, Jonilyn L. Yoder, Terry P. Orlando, Simon Gustavsson, and William D. Oliver. Realization of high-fidelity cz and zz-free iswap gates with a tunable coupler. 11 2020.